Computers and Chemical Engineering 34 (2010) 866–877

Contents lists available at ScienceDirect

Computers and Chemical Engineering

journal homepage: www.elsevier.com/locate/compchemeng

Development of a thermodynamically consistent kinetic model for reactions in the solid oxide fuel cell

P. Vijay, A.K. Samantaray*, A. Mukherjee

Indian Institute of Technology, Kharagpur 721302, India

ARTICLE INFO

Article history:
Received 23 March 2009
Received in revised form
26 November 2009
Accepted 20 December 2009
Available online 29 December 2009

Keywords:
Parameter estimation
Thermodynamic consistency
Reaction kinetics
Solid oxide fuel cell

ABSTRACT

The parameter estimation using the traditional kinetic modeling of complex reaction systems will give incorrect results if the reaction mechanism contains a loop. In this work, a thermodynamically consistent kinetic model of the anodic electrochemical hydrogen oxidation reaction mechanism of a solid oxide fuel cell (SOFC) is formulated. An iterative algorithm for estimating the reaction rate constants using the thermodynamically consistent model formulation is developed. The kinetic parameters estimated using the proposed method gives a better fit to the experimental data. Using the concept of 'Degree of rate control' it is found that the surface reactions may have a greater role in deciding the overall rate. The proposed iterative parameter estimation algorithm developed in this work can also be adapted to other complex chemical and biochemical reaction networks for which the reaction rate constants need to be estimated using the experimental data.

1. Introduction

Reaction kinetics modeling is important in the analysis of chemical and biochemical reaction systems. These models can also be used in the design or modification of chemical reactors to optimize product yield, more efficiently separate products, and eliminate environmentally harmful by-products etc. These models are also used for determining the rate-determining step (RDS) in the complex reaction mechanism (Bessler, 2005; Bieberle & Gauckler, 2002). The parameters (such as reaction rate constants) of the reaction system are usually collected from literature. One drawback of this approach is that these kinetic parameters might contain errors that in turn might introduce some errors into the models. This will make the models thermodynamically inconsistent and hence result in incorrect conclusions. The adjustments in kinetic parameters are always necessary because the rate parameters estimated by various approaches will have their intrinsic uncertainties. These adjustments are carried out by systematic optimization of kinetic parameters against experimental data (Mhadeshwar, Wang, & Vlachos, 2003).

The experimental data may come from electrochemical impedance spectroscopy (EIS) in the case of electrochemical reactions (Bessler, 2005; Bieberle & Gauckler, 2002) or temperature programmed desorption in the case of surface reactions (Mhadeshwar et al., 2003). Near-infrared spectroscopy, short-wavelength near-infrared spectroscopy and ultraviolet visible spectroscopy are also common spectroscopic techniques for monitoring chemical reactions using probes, flow cells and optical fibers (Bijlsma, Boelens, Hoefsloot, & Smilde, 2000).

Several works in the literature deal with the thermodynamics of chemical and biochemical reaction networks far from equilibrium. The thermodynamics of stoichiometric biochemical networks in living systems far from equilibrium was reviewed in Qian and Beard (2005). Incorporating the thermodynamic consistency in micro-kinetic model development for surface reaction mechanisms were discussed in Mhadeshwar et al. (2003). In Bessler, Gewies, and Vogler (2007), Bessler, Warnatz, and Goodwin (2007), and Mhadeshwar et al. (2003) the thermodynamic consistency of the reaction kinetics model was achieved by using the constraints relating the reaction enthalpies and the entropies to the activation energies and the pre-exponential constants respectively. However, for using such an approach, the thermodynamic data for various chemical species participating in the reaction and the reaction intermediates needs to be known, which are not widely available. In Bessler, Warnatz, et al. (2007), the required thermodynamic data was collected from various sources. Because of this, they may have errors in them which may introduce some errors into the models. Further, the thermodynamic data may not be available for all the desired temperatures and pressures. Moreover, this approach is cumbersome if the aim is only to estimate the reaction rate coefficients using the experimental impedance data and not the pre-exponential constants or the activation energies.

* Corresponding author at: Indian Institute of Technology, Mechanical Engineering Department, Systems, Dynamics and Controls Lab, Kharagpur 721302, West Bengal, India. Tel.: +91 3222 282998; fax: +91 3222 282278.
E-mail addresses: vijay103@rediffmail.com (P. Vijay), samantaray@lycos.com (A.K. Samantaray), amalendu@mech.iitkgp.ernet.in (A. Mukherjee).

0098-1354/$ – see front matter © 2009 Elsevier Ltd. All rights reserved.
doi:10.1016/j.compchemeng.2009.12.007

While the kinetic simulations are still possible using thermodynamically inconsistent mechanisms, the results may not be valid (Bessler, Gewies, et al., 2007). Especially, in chemical reaction networks containing cyclic reactions, incorrectly estimated kinetic parameters may lead to the violation of microscopic reversibility (also known as the principle of detailed balance). In the case of chemical reactions, microscopic reversibility means that at thermodynamic equilibrium, the forward rate of the reaction should be equal to the reverse rate and hence the overall flux should be zero. If the estimated parameters make the model of a reaction system consisting of cyclic reactions thermodynamically inconsistent, then cyclic fluxes might occur at equilibrium (Ederer & Gilles, 2007a). In order to overcome these difficulties, thermodynamically feasible, kinetic model of reaction networks, which adopts the concepts of potentials and forces from irreversible thermodynamics, was proposed in Ederer and Gilles (2007a). However, this method requires the knowledge of standard chemical potentials of all the species participating in the reaction mechanism.

Taking the cue from Ederer and Gilles (2007a), the aim of this work is to formulate a thermodynamically consistent reaction kinetic model of the SOFC anodic nickel/yttria-stabilized zirconia (Ni/YSZ) electrochemical reaction mechanism and to develop an algorithm for estimating the parameters (reaction rate constants) by using the developed model. Further, the identification of the rate-determining step (RDS) in the mechanism is attempted using the concept of the 'Degree of rate control' suggested in Campbell (1994).

2. Shortcomings of the traditional reaction kinetics model formulation

Traditionally, the kinetics of chemical and electrochemical reaction mechanisms are modeled by writing the mass balance for the chemical species involved in the reaction. The rate of formation or depletion of a particular species due to a specific reaction is obtained by multiplying the reaction rate with the stoichiometric coefficient of that species in that reaction. The reaction rates are given by rate laws such as the mass action law.

This kind of model formulation has a drawback that the constraints imposed by the thermodynamics are not integrated into the model structure. Using the traditional model formulation for parameter estimation might result in physically infeasible parameter values, which will render the system thermodynamically inconsistent. This is especially the case when the reaction pathway contains a loop. In such a case, non-consideration of the thermodynamic constraints may lead to incorrectly estimated parameters, which will give rise to non-zero flux at thermodynamic equilibrium, thereby violating microscopic reversibility (Onsager, 1931a; Onsager, 1931b). This is illustrated in this section by using an electrochemical hydrogen oxidation mechanism on a Ni/YSZ pattern anode of a SOFC given in Bieberle and Gauckler (2002).

The overall reaction of the hydrogen oxidation on a SOFC anode is given as

$$H_{2(gas)} + O^{2-}_{(electrolyte)} \rightarrow H_2O_{(gas)} + 2e^-_{(electrolyte)}. \quad (1)$$

Although information about the specific reaction steps of the Ni, H_2–H_2O|YSZ system is sparse in the literature (Bieberle & Gauckler, 2002), various reaction mechanisms suggesting a number of different reaction pathways have been proposed. A review of the different reaction mechanisms proposed in literature can be found in Bieberle (2000). The SOFC anode kinetics cannot be understood easily because of complicated, three-dimensionally interconnected microstructure of the anode as well as due to the manifold chemical and electrochemical reactions taking place under SOFC operating conditions. Therefore a simplified microstructure consisting of two-dimensional Ni-YSZ contacts, Ni pattern anode was considered for the kinetic studies in Bieberle and Gauckler (2002). Further, a simple electrochemical model that does not consider all the possible reaction steps at the SOFC anode was considered for demonstrating the proposed state-space modeling approach. In addition, the following assumptions were made. The hydrogen oxidation reaction was assumed to take place on the nickel surface only. Surface diffusion processes of species formed or consumed at the three-phase boundary were neglected. In particular, it is assumed that the oxygen atoms, which are produced through charge transfer reaction at the three-phase boundary, are homogeneously distributed over the active nickel area (*e.g.*, through fast diffusion processes). A single step charge transfer reaction was also assumed.

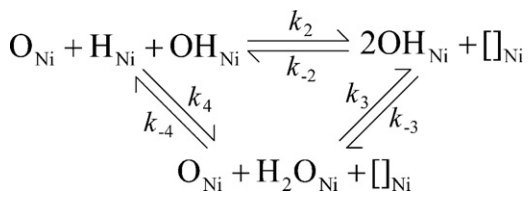

Fig. 1. The loop in the SOFC anodic reaction mechanism.

The same anodic reaction mechanism was considered in Bessler (2005) for demonstrating a new computational approach for SOFC impedance. The same mechanism is considered in this work also, so that the new formulation and the parameter estimation algorithm proposed in this work can be validated by means of comparison with the results from Bieberle and Gauckler (2002) and Bessler (2005). The anodic reaction mechanism consists of a charge transfer reaction, three surface reactions and two adsorption/desorption reactions. Note that the same notations used in Bessler (2005) are also used in this work in order to represent the reaction steps, which are given as

$$O^{\times}_{O(electrolyte)} + []_{Ni} \underset{k_{-1}}{\overset{k_{+1}}{\rightleftharpoons}} O_{Ni} + V^{\bullet\bullet}_{O(electrolyte)} + 2e^-_{(electrode)}, \quad (2)$$

$$O_{Ni} + H_{Ni} \underset{k_{-2}}{\overset{k_{+2}}{\rightleftharpoons}} OH_{Ni} + []_{Ni}, \quad (3)$$

$$O_{Ni} + H_2O_{Ni} \underset{k_{-3}}{\overset{k_{+3}}{\rightleftharpoons}} 2OH_{Ni}, \quad (4)$$

$$OH_{Ni} + H_{Ni} \underset{k_{-4}}{\overset{k_{+4}}{\rightleftharpoons}} H_2O_{Ni} + []_{Ni}, \quad (5)$$

$$H_2O_{(gas)} + []_{Ni} \underset{k_{-5}}{\overset{k_{+5}}{\rightleftharpoons}} H_2O_{Ni}, \quad (6)$$

and

$$H_{2(gas)} + []_{Ni} + []_{Ni} \underset{k_{-6}}{\overset{k_{+6}}{\rightleftharpoons}} H_{Ni} + H_{Ni}, \quad (7)$$

where the forward and reverse reaction rate coefficients are denoted as $k_{\pm 1}$, the subscript '*i*' denotes the reaction number, a free nickel surface site is represented by $[]_{Ni}$, the oxygen ion concentration $O^{\times}_{O(electrolyte)}$ and the concentration of oxygen vacancies $V^{\bullet\bullet}_{O(electrolyte)}$ in the electrolyte are assumed constant and are included into the rate coefficients $k_{\pm 1}$.

The surface reactions (Eqs. (3)–(5)) in the considered reaction pathway of the anodic hydrogen oxidation reaction mechanism forms a loop. This can be shown by adding OH_{Ni} to both sides of Eq. (3); adding $[]_{Ni}$ to both sides of Eq. (4); and by adding O_{Ni} to both sides of Eq. (5). With the above changes, it is seen from Fig. 1 that the surface reactions form a loop. Note that adding the same component on both sides of the reaction, which does not take part in that reaction, does not change the reaction rate or the equilibrium constant.

The second law and detailed balance demands that at thermodynamic equilibrium (Ederer & Gilles, 2007a), the fluxes of all the individual reactions are zero *i.e.*, $J_{2,eq} = J_{3,eq} = J_{4,eq} = 0$, where the 'eq' in the subscript represents the equilibrium quantities. The equilibrium fluxes of the reactions can be given by the law of mass action as

$$J_{2,eq} = k_{+2}c_{O,eq}c_{H,eq} - k_{-2}c_{OH,eq}c_{Ni,eq}, \quad (8)$$

$$J_{3,eq} = k_{+3}c_{O,eq}c_{H_2O,eq} - k_{-3}c_{OH,eq}^2, \quad (9)$$

and

$$J_{4,eq} = k_{+4}c_{H,eq}c_{OH,eq} - k_{-4}c_{H_2O,eq}c_{Ni,eq}. \quad (10)$$

Equating each of the fluxes individually to zero gives the following constraints on the reaction rate constants.

$$\frac{k_{-2}}{k_{+2}} = \frac{c_{O,eq}c_{H,eq}}{c_{OH,eq}c_{Ni,eq}}, \quad (11)$$

$$\frac{k_{+3}}{k_{-3}} = \frac{c_{OH,eq}^2}{c_{O,eq}c_{H_2O,eq}}, \quad (12)$$

and

$$\frac{k_{+4}}{k_{-4}} = \frac{c_{H_2O,eq}c_{Ni,eq}}{c_{H,eq}c_{OH,eq}}. \quad (13)$$

Multiplying both sides of Eqs. (11)–(13), gives rise to the following condition for the reaction rate constants, which is called as the detailed balance relation or the Wegscheider condition (Avetisov, Kuchaev, & Murzin, 2006; Colquhoun, Dowsland, Beato, & Plested, 2004; Ederer & Gilles, 2007a; Onsager, 1931a; Onsager, 1931b; Yang, Bruno, Hlavacek, & Pearson, 2006).

$$Wr = \frac{k_{-2}k_{+3}k_{+4}}{k_{+2}k_{-3}k_{-4}} = 1, \quad (14)$$

where the ratio is denoted by '*Wr*' for convenience. For all other parameter combinations the model describes a physically impossible system with a non-zero equilibrium flux and thus a permanent deviation of the concentrations from the equilibrium ratios (Ederer & Gilles, 2007a).

When the reaction rate constants estimated in Bessler (2005) were substituted into the Wegscheider condition, it was found that the value of the ratio '*Wr*' is 2.8017×10^{-4} instead of 1. Therefore, the reaction rate constants reported in Bessler (2005) makes the system thermodynamically inconsistent. This should result in non-zero equilibrium reaction fluxes for the surface reactions, which is found to be true from the simulations. As the cell is maintained at constant temperature and pressure conditions, application of zero over-voltage between the working and the reference electrodes will result in no reaction taking place and hence no current flow. Therefore, thermodynamic equilibrium in this case implies that the applied over-voltage is zero. Application of zero over-voltage to the dynamic model resulted in non-zero reaction fluxes for the surface reactions ($J_{2,eq}$, $J_{3,eq}$ and $J_{4,eq}$), while it gave zero fluxes ($J_{3,eq}$ and $J_{4,eq}$) for the charge transfer and the adsorption/desorption reactions.

Further, the driving forces and fluxes in the dynamic system are not explicitly considered in the traditional reaction kinetics formulation. If the driving forces and fluxes are integrated into the structure of the model, then their sign equivalence will alone ensure that thermodynamics is not violated (Ederer & Gilles, 2007a). If the traditional formulation of the reaction kinetics is used for estimating the reaction rate constants it may lead to violation of the second law and the principle of detailed balance. It can be seen from Eqs. (8)–(10) that, if the reaction rate constants ($k_{\pm 1}$'s) are allowed to be individually varied (during the parameter estimation), the reaction fluxes (J_i's) can either be positive or negative irrespective of the sign of the driving forces (change in the Gibbs free energies ($(\Delta G)_i$'s)). It might so happen that the reaction fluxes become positive even if the driving forces are negative, which leads to violation of the second law of thermodynamics. In the case of cyclic reactions, the opposing signs of the driving force and the flux will lead to non-zero flux at thermodynamic equilibrium thus violating microscopic reversibility.

3. Traditional modeling of the anodic SOFC electrochemical reaction mechanism

The electrochemical information of fuel cell electrode surface reaction mechanisms are usually obtained from the experimental electrochemical impedance spectroscopy (EIS) results by means of fitting this data to equivalent circuits (Bessler, 2005; Bieberle & Gauckler, 2002; Macdonald, 1987). This method, although quite popular, suffers from the disadvantage that the correlation of the equivalent circuit elements with the physical and chemical parameters is not straightforward (Bieberle & Gauckler, 2002). In order to overcome these difficulties, a state-space modeling approach for modeling the anodic reaction system in a SOFC was proposed by Bieberle (2000), Bieberle and Gauckler (2002), Mitterdorfer and Gauckler (1998), Mitterdorfer and Gauckler (1999a) and Mitterdorfer and Gauckler (1999b). Later, a computational approach for calculating the impedance from the time domain transient simulations that maintains the full non-linear response was proposed in Bessler (2005).

In this section, the traditional method followed for modeling of the electrochemical reaction kinetics, which was adopted in Bessler (2005) for modeling the anodic SOFC reaction system, is briefly described.

The differential equations of the system are formulated in terms of the fractions of surface coverages of the different surface species (O, H, OH and H_2O), which are defined as

$$\theta_j = \frac{c_j}{N_0}, \quad (15)$$

where c_j is the number of nickel surface sites where the species '*j*' is adsorbed and N_0 is the total number of nickel surface sites. The fraction of surface coverage of each species must adopt values between 0 and 1. The total surface coverage, which is the sum of the fractions of all surface coverages, must be smaller than one. The surface coverage fraction of free sites on the nickel surface is therefore given as

$$\theta_{Ni} = 1 - (\theta_H + \theta_O + \theta_{OH} + \theta_{H_2O}). \quad (16)$$

The rates of the reactions (J_i's) can be obtained by using the law of mass action. From the reaction rates, the rate equations for all the surface species may be obtained as (Bessler, 2005):

$$\frac{d\theta_O}{dt} = J_1 - J_2 - J_3 = k_{+1}\theta_{Ni} - k_{-1}\theta_O - k_{+2}\theta_O\theta_H + k_{-2}\theta_{OH}\theta_{Ni} - k_{+3}\theta_O\theta_{H_2O} + k_{-3}\theta_{OH}^2. \quad (17)$$

$$\frac{d\theta_H}{dt} = -J_2 - J_4 + 2J_6 = -k_{+2}\theta_O\theta_H + k_{-2}\theta_{OH}\theta_{Ni} - k_{+4}\theta_H\theta_{OH} + k_{-4}\theta_{H_2O}\theta_{Ni} + 2k_{+6}\theta_{Ni}^2 - 2k_{-6}\theta_H^2. \quad (18)$$

$$\frac{d\theta_{OH}}{dt} = J_2 + 2J_3 - J_4 = k_{+2}\theta_O\theta_H - k_{-2}\theta_{OH}\theta_{Ni} + 2k_{+3}\theta_O\theta_{H_2O} - 2k_{-3}\theta_{OH}^2 - k_{+4}\theta_H\theta_{OH} + k_{-4}\theta_{H_2O}\theta_{Ni}. \quad (19)$$

$$\frac{d\theta_{H_2O}}{dt} = -J_3 + J_4 + J_5 = -k_{+3}\theta_O\theta_{H_2O} + k_{-3}\theta_{OH}^2 + k_{+4}\theta_H\theta_{OH} - k_{-4}\theta_{H_2O}\theta_{Ni} + k_{+5}\theta_{Ni} - k_{-5}\theta_{H_2O}. \quad (20)$$

The differential equations of the reaction system can be expressed in matrix notations as

$$\begin{Bmatrix} \frac{d\theta_O}{dt} \\ \frac{d\theta_H}{dt} \\ \frac{d\theta_{OH}}{dt} \\ \frac{d\theta_{H_2O}}{dt} \end{Bmatrix} = \begin{bmatrix} 1 & -1 & -1 & 0 & 0 & 0 \\ 0 & -1 & 0 & -1 & 0 & 2 \\ 0 & 1 & 2 & -1 & 0 & 0 \\ 0 & 0 & -1 & 1 & 1 & 0 \end{bmatrix} \begin{Bmatrix} J_1 \\ J_2 \\ J_3 \\ J_4 \\ J_5 \\ J_6 \end{Bmatrix}, \quad (21)$$

where the 4×6 matrix is called as the stoichiometric matrix denoted by **S**. The reaction rate coefficients for all the reactions except the charge transfer reaction are considered constants for the given cell temperature and pressures of the gas species (hydrogen and water vapour). The reaction rate coefficients for the charge transfer reaction are functions of temperature, activation energy and over-voltage. The terms which are dependent on the temperature and activation energy are grouped into a constant term, $k_{\pm1}^0$. The other over-voltage dependant parts are constant for a constant value of over-voltage, but are time dependent for time dependent variations in the over-voltage. The reaction rate coefficients for the single step charge transfer are given as (Bessler, 2005; Bockris & Reddy, 1973):

$$k_{+1} = k_{+1}^0 \exp\left(\beta \frac{zF}{RT}\eta\right) \quad (22)$$

and

$$k_{-1} = k_{-1}^0 \exp\left(-(1-\beta)\frac{zF}{RT}\eta\right). \quad (23)$$

Harmonically varying over-voltage (η), which is applied to the cell during the experiment, is considered as input to the model in order to calculate the impedance.

$$\eta(t) = \eta_{steady} + \eta_{var}\sin(\omega t), \quad (24)$$

where η_{steady} represents the steady state polarization over-voltage, which is taken as 0 V and η_{var} is the amplitude of the periodically varying component.

The rate equations for the surface species (Eqs. (17)–(20)), along with the boundary condition in Eq. (16), form a differential algebraic equation system, which can be numerically integrated to obtain the time varying surface coverages of the surface species. The resulting time varying Faradaic current $i(t)$ is obtained from the net rate of the charge transfer and is given by (Bessler, 2005; Bockris & Reddy, 1973):

$$i(t) = zF\Gamma A f_{geo}(k_{+1}(t)\theta_{Ni}(t) - k_{-1}(t)\theta_O(t)), \quad (25)$$

where Γ (in mol cm^{-2}) is the area density of the surface sites on a microscopic scale, A (cm^2) is the total (macroscopic) surface area of the electrode and f_{geo} is a dimensionless geometrical factor, which is the only electrode structural parameter defined as the ratio of active microscopic surface area and total macroscopic surface area A. It is correlated with both the three-phase boundary length and active electrode width (Bessler, 2005).

The method used in laboratory frequency response analyzers for data evaluation was used for impedance calculation in Bessler (2005). The real and imaginary parts of the complex admittance ($Y = Y' + jY''$) are given as (Bessler, 2005):

$$Y' = \frac{i_1 A f_{geo}}{\eta_{var}}\cos(\phi) = \frac{2A f_{geo}}{\eta_{var}\tau}\int_{t=0}^{\tau} i(t)\sin(\omega t)\,dt \quad (26)$$

and

$$Y'' = \frac{i_1 A f_{geo}}{\eta_{var}}\sin(\phi) = \frac{2A f_{geo}}{\eta_{var}\tau}\int_{t=0}^{\tau} i(t)\cos(\omega t)\,dt. \quad (27)$$

where $\tau = 2\pi/\omega$ is the time period of the output oscillations. The impedance is obtained as the inverse of the admittance as

$$Z = Y^{-1}. \quad (28)$$

The model parameters were estimated by varying their values until a best agreement between the simulation results and the experimental data is obtained (which is referred to as 'fitting'). The fitting was done using a Lavenberg–Marquardt non-linear least squares algorithm.

4. Thermodynamically consistent reaction kinetics model formulation

A problematic aspect with the traditional reaction kinetics models given in Eqs. (15)–(28) is that it does not explicitly consider the driving forces of the reactions. Model equations for electrical and mechanical systems explicitly contain voltages and forces, which are physical quantities driving electrical current and displacement changes respectively; *i.e.*, fluxes and conjugated forces point in the same direction. In the case that no external forces are imposed to the system this guarantees the existence of an equilibrium state where all forces and fluxes are zero. Thus the fulfillment of the second law and of detailed balance is ensured by the model structure and it is not necessary to observe special detailed balance equations for the parameters (Ederer & Gilles, 2007a).

The quantities usually considered as potentials and driving forces of chemical reaction systems (chemical potentials and Gibbs free energies respectively) are quite unsuited for kinetic modeling far from equilibrium (Ederer & Gilles, 2007a). This is because; the reaction resistance in this case is not a constant but a complex non-linear function of the concentrations (refer to Appendix A). Further, the values of the standard chemical potentials of all the species involved in the reaction mechanism are required for formulating the model using the above power variables, which are not widely available in literature. For this purpose, a new thermo-kinetic force was proposed in Ederer and Gilles (2007a), which conserves the sign dependence of the force on the concentrations. Taking the cue from this work, the thermo-kinetic formulation for a general surface reaction, in terms of surface coverage fractions, is given in Appendix B. The differential equations of the SOFC anodic hydrogen oxidation reaction mechanism are rewritten using this revised formulation as

$$\frac{d\theta_O}{dt} = \frac{e_f}{R_1}\frac{\theta_{Ni}}{\Theta_{Ni}} - \frac{e_r}{R_1}\frac{\theta_O}{\Theta_O} - \frac{1}{R_2}\frac{\theta_O\theta_H}{\Theta_O\Theta_H} + \frac{1}{R_2}\frac{\theta_{OH}\theta_{Ni}}{\Theta_{OH}\Theta_{Ni}} - \frac{1}{R_3}\frac{\theta_O\theta_{H_2O}}{\Theta_O\Theta_{H_2O}} + \frac{1}{R_3}\frac{\theta_{OH}^2}{\Theta_{OH}^2}. \quad (29)$$

$$\frac{d\theta_H}{dt} = -\frac{1}{R_2}\frac{\theta_O\theta_H}{\Theta_O\Theta_H} + \frac{1}{R_2}\frac{\theta_{OH}\theta_{Ni}}{\Theta_{OH}\Theta_{Ni}} - \frac{1}{R_4}\frac{\theta_H\theta_{OH}}{\Theta_H\Theta_{OH}} + \frac{1}{R_4}\frac{\theta_{H_2O}\theta_{Ni}}{\Theta_{H_2O}\Theta_{Ni}} + \frac{2}{R_6}\frac{\theta_{Ni}^2}{\Theta_{Ni}^2} - \frac{2}{R_6}\frac{\theta_H^2}{\Theta_H^2}. \quad (30)$$

$$\frac{d\theta_{OH}}{dt} = \frac{1}{R_2}\frac{\theta_O\theta_H}{\Theta_O\Theta_H} - \frac{1}{R_2}\frac{\theta_{OH}\theta_{Ni}}{\Theta_{OH}\Theta_{Ni}} + \frac{2}{R_3}\frac{\theta_O\theta_{H_2O}}{\Theta_O\Theta_{H_2O}} - \frac{2}{R_3}\frac{\theta_{OH}^2}{\Theta_{OH}^2} - \frac{1}{R_4}\frac{\theta_H\theta_{OH}}{\Theta_H\Theta_{OH}} + \frac{1}{R_4}\frac{\theta_{H_2O}\theta_{Ni}}{\Theta_{H_2O}\Theta_{Ni}}. \quad (31)$$

$$\frac{d\theta_{H_2O}}{dt} = -\frac{1}{R_3}\frac{\theta_O\theta_{H_2O}}{\Theta_O\Theta_{H_2O}} + \frac{1}{R_3}\frac{\theta_{OH}^2}{\Theta_{OH}^2} + \frac{1}{R_4}\frac{\theta_H\theta_{OH}}{\Theta_H\Theta_{OH}} - \frac{1}{R_4}\frac{\theta_{H_2O}\theta_{Ni}}{\Theta_{H_2O}\Theta_{Ni}} + \frac{1}{R_5}\frac{\theta_{Ni}}{\Theta_{Ni}} - \frac{1}{R_5}\frac{\theta_{H_2O}}{\Theta_{H_2O}}. \quad (32)$$

The terms e_f and e_r in Eq. (29) represent the time varying over-voltage dependant exponential terms of the reaction rate coefficients of the charge transfer reaction (refer to Eqs. (22) and (23)) and they are given by

$$e_f = \exp\left(\beta\frac{zF}{RT}\eta\right) \quad (33)$$

and

$$e_r = \exp\left(-(1-\beta)\frac{zF}{RT}\eta\right). \quad (34)$$

The time dependent input over-voltage is given by Eq. (24) and the output current is calculated using Eq. (25). The same procedure given in Section 3 is used for calculating the impedance from the time dependent input and output (refer to Eqs. (26)–(28)).

The values of the capacities (Θ_j's) for the different species are required for performing the simulations and for the parameter estimation using the new formulation. The capacities of the various species involved in the reaction system can be directly calculated (refer to Eqs. (47) and (48) in Appendix B) if their standard chemical potentials ($\mu_{j,0}$'s) are known. But such data are unavailable in the literature. However, it is shown in Appendix B that any set of equilibrium concentrations of the system can be used as capacities.

The rate equations (Eqs. (29)–(32)) along with the boundary condition given in Eq. (16) form the new formulation of the SOFC anodic reaction kinetics. Since the rank of the stoichiometric matrix **S** (refer to Eq. (21)) is 4, the four linearly independent algebraic equations (steady state forms of Eqs. (17)–(20) with $\eta = 0$), can be used to solve for the equilibrium surface coverage fractions of the surface species (O, H, OH and H_2O), which can be used as capacities (refer to Eq. (56) in Appendix B). The equilibrium surface coverage fractions can be obtained by solving the equilibrium model (steady state forms of Eqs. (17)–(20), after substituting Eq. (16) into those equations and putting $\eta = 0$), provided that the values of all the reaction rate constants ($k_{\pm i}$'s) are known. The equilibrium surface coverage fraction of empty Ni sites ($\theta_{Ni,eq}$) follows from Eq. (16).

It can be seen that for a given set of values of the reaction rate constants ($k_{\pm i}$'s) and the corresponding set of values of capacities (Θ_j's) calculated from the equilibrium model, the differential equations of the new formulation (Eqs. (29)–(32)) are the same as the equations resulting from the traditional formulation (Eqs. (17)–(20)). Therefore, for such a case, the simulation results will be the same for both the formulations.

This new formulation ensures that the constraint given in Eq. (54) in Appendix B is imposed on all the reactions in the system, thereby satisfying the Wegscheider condition if the reaction system contains cycles. Estimation of R_i's in the new formulation instead of $k_{\pm i}$'s in the traditional formulation also ensures that $\text{sign}(F_d)_i = \text{sign}(\Delta G)_i = \text{sign}\, J_i$ for all values of R_i. This is because of the fact that the values chosen for R_i are all positive, which requires that the sign of J_i be equal to the sign of $(F_d)_i$ (refer to Eq. (52) in Appendix B). Therefore observance of the second law of thermodynamics and detailed balance are assured with this revised formulation. The thermodynamic consistency condition for the chemical reaction system far from equilibrium is given by the De Donder equation (Boudart, 2001; Campbell, 2001; Dumesic, 1999; Fishtik, Callaghan, Fehribach, & Datta, 2005; Fishtik & Datta, 2001; Holstein & Boudart, 1997), which defines the far from equilibrium relation between the forward and reverse reaction fluxes (J_{+i} and J_{-i} respectively). It is shown in Appendix B that the new formulation satisfies the De Donder relations.

The advantage of this new formulation is that the thermodynamic constraints are integrated into the model structure and hence avoids the detailed test of the parameters for thermodynamic consistency, which requires extensive thermodynamic data. Another advantage of the new formulation is that the optimization algorithm using the new formulation will not spend time in examining impossible parameter sets (due to the constraint embedded into the system), and hence the search space and time are reduced. Further, the number parameters in the system is reduced from 12 ($k_{\pm i}$'s) in the traditional formulation to 6 (R_i's) in the new one.

5. Parameter estimation procedure using the new formulation

In this section, an iterative procedure for estimating the parameters (reaction rate constants) using the new model formulation is presented. This procedure exploits the relation between the reaction rate constants and the set of capacities (which are equal to the set of equilibrium surface fractions) of a reaction (refer to Eqs. (54) and (56) in Appendix B) and also uses the Wegscheider condition, which defines the condition for thermodynamic consistency of the reaction network having a loop. It also uses the equilibrium model defined in Section 4.

As the exact values of the capacities are not known, it is not possible to estimate the reaction rate constants in a single iteration. Therefore, in this work, an iterative parameter estimation procedure is proposed for estimating the reaction rate constants using the new model formulation, which results in parameters that do not violate the thermodynamic consistency of the model.

If the exact values of the capacities are known (say from the measurement of equilibrium concentrations), we can expect to attain the exact values of the reaction rate constants (refer to Eqs. (47) and (48) in Appendix B), which satisfy the Wegscheider condition (and hence maintain the thermodynamic consistency of the system) without resorting to recursive calculations. This is because, the estimation of R_i's using the new formulation imposes the constraint given in Eq. (54) in Appendix B on the reaction rate constants ($k_{\pm i}$'s) of the individual reactions of the system, thereby resulting in satisfaction of the Wegscheider condition and microscopic reversibility.

But, if the capacities are not known, the parameter estimation is done using the set of values of capacities obtained by solving the equilibrium model with the reaction rate constants from literature (which violate the Wegscheider condition). The $k_{\pm i}$'s corresponding to the estimated R_i's are calculated using the capacity values in Eq. (54) in Appendix B. Though these $k_{\pm i}$'s satisfy Eq. (54), they need not necessarily satisfy the Wegscheider condition. This is because the capacities used are not the true equilibrium surface coverage fractions that define the equilibrium constants of the reactions. But we can expect the new reaction rate constants to give a better value of the ratio of '*Wr*' (*i.e.*, more closer to one). This is because, the integration of Eq. (54) into the new formulation introduces a constraint in the search space, which despite the approximate values of the capacities, guides the search in a favorable direction (*i.e.*, towards the parameters that satisfy the Wegscheider conditions). This can be checked by applying the Wegscheider condition to the reaction rate constants (the new values must give better results).

Now that better values of the reaction rate constants are obtained, they can be used to calculate new set of capacities by solving the equilibrium model, which will be closer to the actual equilibrium surface coverage fractions. The resulting capacities are then used for again estimating the R_i's and hence the $k_{\pm i}$'s. In this fashion, the calculations are performed iteratively until a parameter

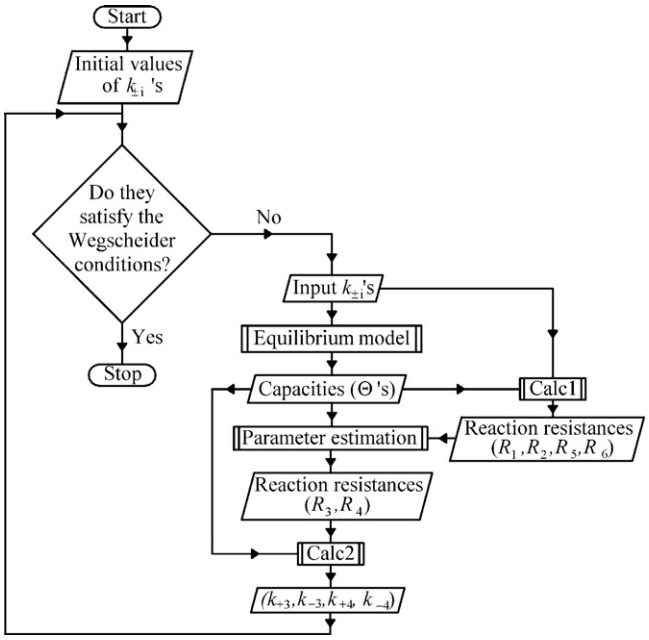

Fig. 2. Flow chart of the recursive procedure for parameter estimation using the proposed formulation.

set is obtained which satisfies the Wegscheider condition exactly. Thus, this procedure effectively fits not only the reaction resistances but also the capacities to the experimental data, thereby resulting in parameter estimates, which do not cause the model to violate the laws of thermodynamics.

The recursive procedure developed for estimating the reaction rate constants subject to the thermodynamic constraints using the new model formulation is given in the form of a flow chart in Fig. 2.

For the specific SOFC anodic electrochemical reaction mechanism considered in this work, the values of reaction rate constants were presented in Bieberle and Gauckler (2002). Some of those parameter values were collected from various literatures, while others were calculated using physical relations. Starting from the values of parameters in Bieberle and Gauckler (2002), the parameters k_{-2}, k_{-3} and k_{-5} were estimated in Bessler (2005), as those parameter values seemed to be uncertain in the literature. The parameter set (reaction rate constants) taken from the results of Bessler (2005) is given in Table 1. These parameters are taken as the starting values in this work.

In order to identify which reaction rate constants cause the error in the Wegscheider condition, the reaction resistances for all the reactions are calculated using the relation given in Eq. (54) in Appendix B. For this purpose, the capacities are calculated by solving the equilibrium model with the parameters given in Table 1. It is found that the values of the reaction resistances calculated using the forward and reverse reaction rate constants do not match for

Table 1
Reaction rate constants from Bessler (2005).

	k_{+i} (s^{-1})	k_{-i} (s^{-1})
k_1^0	2.0×10^2	5.6×10^{10}
k_2	2.0×10^{11}	1.3×10^4
k_3	1.0×10^{12}	5.8×10^2
k_4	1.5	6.0×10^5
k_5	8.0×10^4	1.0×10^{11}
k_6	6.0×10^7	2.4×10^8

the reactions given in Eqs. (4) and (5), which means that the constraint in Eq. (54) in Appendix B is not satisfied by the corresponding reaction rate constants. Therefore, the corresponding reaction rate constants (k_{+3}, k_{-3}, k_{+4} and k_{-4}) are identified to be the ones that cause the error in the Wegscheider condition. The reaction resistances for those two reactions (R_3 and R_4) are chosen to be the ones to be estimated by the parameter estimation algorithm using the newly formulated model.

A code is written in Matlab for solving the equilibrium model *i.e.*, the non-linear algebraic equations which are the steady state forms of Eqs. (17)–(20) into which Eq. (16) is substituted and $\eta = 0$. This is denoted by the predefined process 'Equilibrium state model' in Fig. 2. This equilibrium model gives the equilibrium surface coverage fractions which are used as capacities.

Another Matlab code is written, which solves the algebraic differential equation system of the new formulation in order to obtain the time varying current response. The impedance is then calculated for various frequencies using Eqs. (26)–(28). These impedance values along with the experimental impedance values are then used for estimating the unknown parameters (R_3 and R_4). The procedure for estimating the reaction resistances R_3 and R_4, which is represented by the predefined process 'parameter estimation' shown in Fig. 2, is given as follows:

(1) The initial estimates of the reaction resistances, R_3 and R_4 are provided to the parameter estimation algorithm. Also the values of the Θ_j's obtained by solving the equilibrium model (using the parameters given in Table 1 for the first iteration) are provided as inputs to the algorithm. Other parameter values used are given in Table 2.
(2) A value of the frequency of the sinusoidal varying over-voltage is chosen for which, the experimental impedance data is available. For that input frequency, solve the differential equation system given in Eqs. (29)–(32) using the stiff ordinary differential equation solver 'ode15s' available in Matlab. The simulation is run for sufficiently long time so that the transients die out and the dynamic steady state is reached. The time varying surface coverage fractions for the different surface species involved in the system ($\theta_H, \theta_H, \theta_{OH}, \theta_{H_2O}$ and θ_{Ni}) are obtained from the simulations. The time varying output current is calculated using Eq. (25).

Table 2
Other parameters used in the simulation (from Bessler, 2005).

Symbol	Description	Value	Unit
T	Absolute temperature	973	K
f_{geo}	Geometric factor	0.37	–
Γ	Nickel surface site density	1.67×10^{-9}	mol cm^{-2}
A	Electrode surface area	1	cm^{-2}
z	Number of electrons participating in the reaction	2	–
η_{var}	Amplitude of input sinusoidal over-voltage	10	mV
η_{steady}	Steady state polarization over-voltage	0	mV
F	Faraday's constant	96,500	C mol^{-1}
R	Universal gas constant	8.3141	J mol^{-1} K^{-1}
β	Symmetry factor	0.5	–

(3) Using the time varying current data generated over one cycle, the impedance is calculated using Eqs. (26)–(28). The numerical integration is performed using the Matlab function 'trapz', which uses the trapezoidal method.
(4) Repeat the procedure described in steps 2 and 3 for all other values of the frequencies for which the experimental impedance data are available.
(5) Find the values of the parameters (R_3 and R_4) that minimize the complex least squares error between the experimental impedances and the impedances obtained from the simulations. The 'fminsearch' function available in Matlab is utilized for this purpose.

The predefined process 'parameter estimation' shown in Fig. 2 requires two sets of inputs (the equilibrium surface coverage fractions (Θ_j's) and the reaction resistances (R_1, R_2, R_5 and R_6)), along with the initial guess values for the resistances, R_3 and R_4. Using these inputs, the parameter estimation algorithm estimates the values of R_3 and R_4, which minimize the least squares error between the experimental and the simulated impedances. Note that the output of the process is obtained only after receiving both the inputs. The predefined processes 'Calc1' and 'Calc2', shown in Fig. 2 also require two sets of inputs. Both input sets are required to be fed to those processes before the calculations can be performed and the output obtained.

The predefined process named as 'calc1' in Fig. 2 calculates the values of the reaction resistances R_1, R_2, R_5 and R_6 from the corresponding reaction rate constants and capacities using relations given in Eq. (54) in Appendix B. The reaction resistances estimated by the parameter estimation algorithm (R_3 and R_4) are converted into the reaction rate constants using relations in Eq. (54) by the predefined process 'calc2'.

Note that although only the reaction rate constants corresponding to the surface reactions (k_{+2}, k_{-2}, k_{+3}, k_{-3}, k_{+4} and k_{-4}), which form a loop are required by the decision making step shown in Fig. 2, all the reaction rate constants are required to be input to the equilibrium model in the next step.

6. Degree of rate control

One of the applications of the reaction kinetics models is the determination of the RDS in a multi-step reaction mechanism. However, the definition of the RDS and how to determine which step it is in a complex mechanism are still subject to some controversy (Campbell, 1994; Campbell, 2001). Various suggestions have been given in the literature for determining the RDS (Boudart & Tamaru, 1991; Campbell, 1994; Campbell, 2001; Dumesic, 1999; Fishtik & Datta, 2001) in chemical reaction mechanisms. In Bieberle and Gauckler (2002) it was suggested that the charge transfer reaction might be the RDS for the SOFC anodic electrochemical reaction mechanism because the reaction rate constant for the electronation process was very small. In Bessler (2005), it was suggested that the adsorption/desorption reactions might be rate determining because the polarization resistance and the high frequency impedance are more sensitive to the changes in the corresponding reaction rate constants.

In this work, we adopt the method suggested in Campbell (1994) for determining the RDS. The usefulness of the method suggested in Campbell (1994) for identifying the RDS in models describing various types of multi-step reaction mechanisms was discussed in Baranski (1999). The relation between the overall reaction rate and the velocity of the RDS was also clarified. The method suggested in Campbell (1994) for determining the RDS is a type of sensitivity analysis in which both the forward and the reverse rate constants are increased by 1% (thus not changing its equilibrium constant) and calculating the resulting fractional increase in the overall rate. Then, the most rate-controlling step is the one whose increase leads to the greatest increase in overall rate, J_O. The degree of rate control for the step 'i' is defined in Campbell (1994) as

$$X_i = \left(\frac{k_i}{J_O}\right)\left(\frac{\delta J_O}{\delta k_i}\right) \tag{35}$$

If the change in k_i is small enough so that the system remains linear, then the degree of rate control, X_i, should be a number between zero and one. The rate-controlling step is defined as a step with non-zero X_i. In the case of the SOFC anodic electrochemical reaction mechanism, the overall rate of the anodic reaction is the charge flow rate or current. Also, the reaction resistances (R_i's), which are defined in this work for all the reactions, serve as convenient and physically meaningful variables for performing the sensitivity analysis (Ederer & Gilles, 2007a). A decrease in the value of R_i by 1% for a reaction means that both the forward and the reverse reaction rate constants ($k_{\pm i}$'s) for the reaction are increased by 1% (refer to Eq. (54) in Appendix B), thereby maintaining the k_{eq} constant. Therefore, the degree of rate control is defined in this work in terms of the reaction resistance and current as

$$X_i = \left(\frac{R_i}{i}\right)\left(\frac{\delta i}{\delta R_i}\right). \tag{36}$$

Therefore, the new formulation provides a more intuitive and elegant way of performing the sensitivity analysis for determining the RDS. It is hoped that this definition of the degree of rate control will help in identifying the RDS in the anodic Ni, H_2–H_2O|YSZ reaction mechanism unambiguously.

7. Results and discussion

The calculations for estimating the values of the reaction rate constants are performed in a recursive manner as given in Fig. 2. The '*Wr*' values close enough to one were obtained in two iterations. The reaction rate constants reported in Bessler (2005), which are given in Table 1 are taken as the initial estimates for the iterative procedure. These parameters are substituted into the equilibrium model to get the equilibrium values of the surface coverage fractions which will serve as the capacities required for the new formulation. The values of the equilibrium surface coverage fractions (capacities) of the surface species obtained are $\Theta_O = 2.3384 \times 10^{-9}$, $\Theta_H = 0.3273$, $\Theta_{OH} = 1.7967 \times 10^{-2}$, $\Theta_{H_2O} = 5.2375 \times 10^{-7}$ and $\Theta_{Ni} = 0.6547$. These values along with the values of reaction resistances are supplied as inputs to the parameter estimation algorithm, which uses the new model formulation. The values of reaction resistances estimated by the parameter estimation algorithm are $R_3 = 6.0195$ s and $R_4 = 6.6993$ s. The corresponding values of the reaction rate constants are $k_{+3} = 1.3564 \times 10^{14}\ s^{-1}$, $k_{-3} = 5.1463 \times 10^{2}\ s^{-1}$, $k_{+4} = 25.3803\ s^{-1}$ and $k_{-4} = 4.3533 \times 10^{5}\ s^{-1}$. Substituting these reaction rate constants into the Wegscheider condition gave a value of 1.001146 for '*Wr*'. The closeness of the '*Wr*' to one, shows that the equilibrium surface coverage fractions used in the first iteration of the parameter estimation procedure are not much deviant from the actual values.

Although this looks satisfactory, an attempt was made to add more precision to the results. Therefore, a second iteration was performed. The values of the capacities obtained in the second iteration are $\Theta_O = 2.3381 \times 10^{-9}$, $\Theta_H = 0.3273$, $\Theta_{OH} = 1.7985 \times 10^{-2}$, $\Theta_{H_2O} = 5.2374 \times 10^{-7}$ and $\Theta_{Ni} = 0.6547$. The values of reaction resistances estimated by the parameter estimation algorithm in the second iteration are $R_3 = 5.4197$ s and $R_4 = 7.5517$ s. The corresponding values of the reaction rate constants are $k_{+3} = 1.5068 \times 10^{14}\ s^{-1}$, $k_{-3} = 5.7041 \times 10^{2}\ s^{-1}$, $k_{+4} = 22.4927\ s^{-1}$ and $k_{-4} = 3.8620 \times 10^{5}\ s^{-1}$. Substituting these reaction rate constants into the Wegscheider

Table 3
The reaction rate constants resulting from this work.

	k_{+i} (s^{-1})	k_{-i} (s^{-1})
k_1^0	2.0×10^2	5.6×10^{10}
k_2	2.0×10^{11}	1.3×10^4
k_3	[a] 1.5068×10^{14}	[a] 5.7041×10^2
k_4	[a] 22.4927	[a] 3.8620×10^5
k_5	8.0×10^4	1.0×10^{11}
k_6	6.0×10^7	2.4×10^8

[a] Parameters obtained from the optimization.

condition gave a value of 1.000006. The set of reaction rate constants resulting from this work is presented in Table 3. These values of the reaction rate constants are estimated within the framework of the thermodynamic consistency of the system and hence they are expected to give impedance values much closer to the experimental results.

The Bode magnitude and phase plots obtained from the simulation of this work and those obtained from experiments are compared in Fig. 3a and b. It can be seen from the Bode magnitude plot that the magnitudes obtained from the experiment and the simulation match at very low and very high frequencies. There is a mismatch only at the intermediate frequencies. A high frequency mismatch in the magnitude curve was reported in Bieberle and Gauckler (2002) whereas a low frequency mismatch was reported in Bessler (2005).

The peak in the Bode phase plot obtained from the simulations is offset to the left when compared to the experimental Bode phase plot as shown in Fig. 3b. The simulated Bode phase plot was a little offset to the right in the case of Bieberle and Gauckler (2002) and it was a little offset to the left in the case of Bessler (2005). The maximum phase is the same in all the plots obtained from simulations in Bieberle and Gauckler (2002), Bessler (2005) and this work. The maximum phase shift occurs at around 50 Hz, which the same result is reported in Bessler (2005).

The Nyquist plots obtained using the parameters estimated in this work are compared with the experimental ones and also the ones obtained from the simulation in Bieberle and Gauckler (2002) and Bessler (2005) in Fig. 3c. The Nyquist plot obtained from the simulations in this work lies between the simulated Nyquist plots given in Bieberle and Gauckler (2002) and Bessler (2005) as shown in Fig. 3c. The relaxation frequency obtained from the experimental Nyquist plot is 1 Hz. The relaxation frequency obtained from this work is 3 Hz, which is same as that reported in Bessler (2005). A very high relaxation frequency of 58 Hz was reported in Bieberle and Gauckler (2002). The least squares error between the simulated and the experimental impedance data is $8.1536 \times 10^6\ \Omega^2$ and $3.2376 \times 10^6\ \Omega^2$ in Bieberle and Gauckler (2002) and Bessler (2005) respectively. The least squares error calculated using the data from the simulations in this work is $2.9926 \times 10^6\ \Omega^2$. The parameter's estimations of this work might be better because they give the minimum least squares error between the experimental and the simulated impedances. However, still there is a large deviation between the experimental impedance curve and the one obtained from the simulations. This was attributed to the non-inclusion of a low frequency process (typically a diffusion process) in the model in Bessler (2005). This aspect must be further investigated through more experiments and simulations.

The steady state dynamic response of the system (surface coverage fractions of the surface species and the current) to the sinusoidal varying input over-voltage is shown in Fig. 4 for various input frequencies. The surface coverage fractions of O and OH vary 25% about their steady state values for 1 Hz and 100 Hz input frequencies. The surface coverage fractions of H and H_2O vary 4%

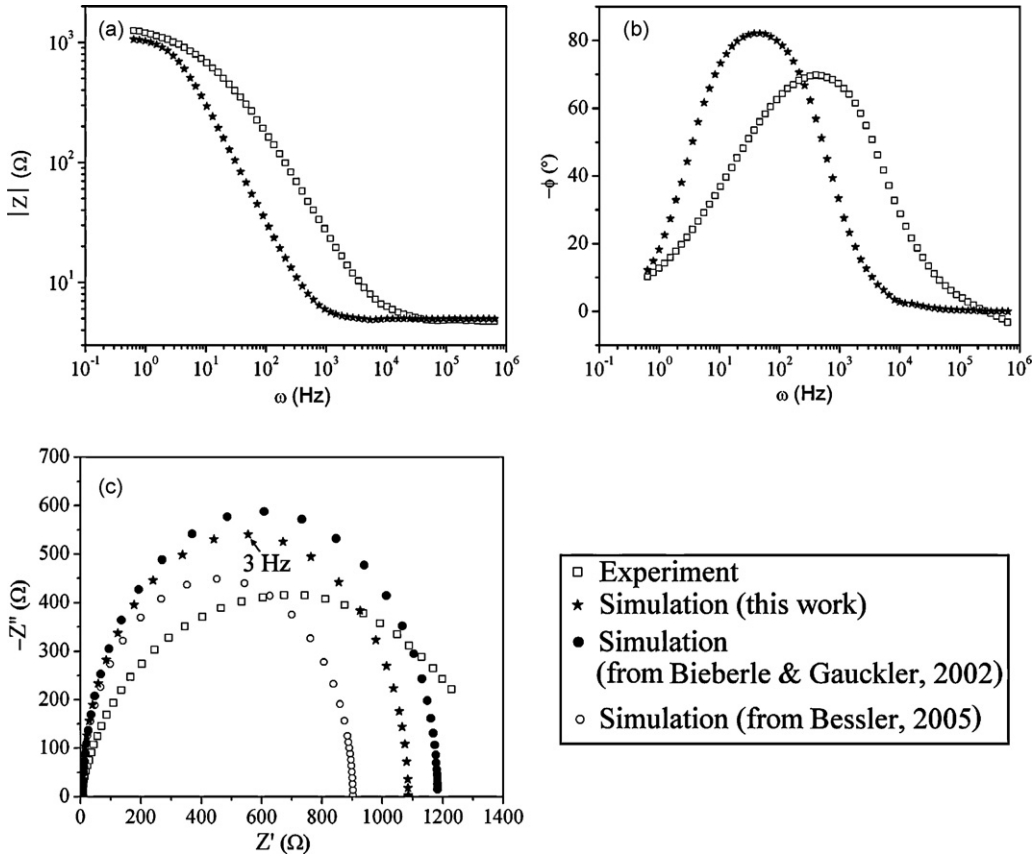

Fig. 3. Comparison between the experimental and simulated impedances: (a) Bode magnitude plot, (b) Bode phase plot and (c) Nyquist plot.

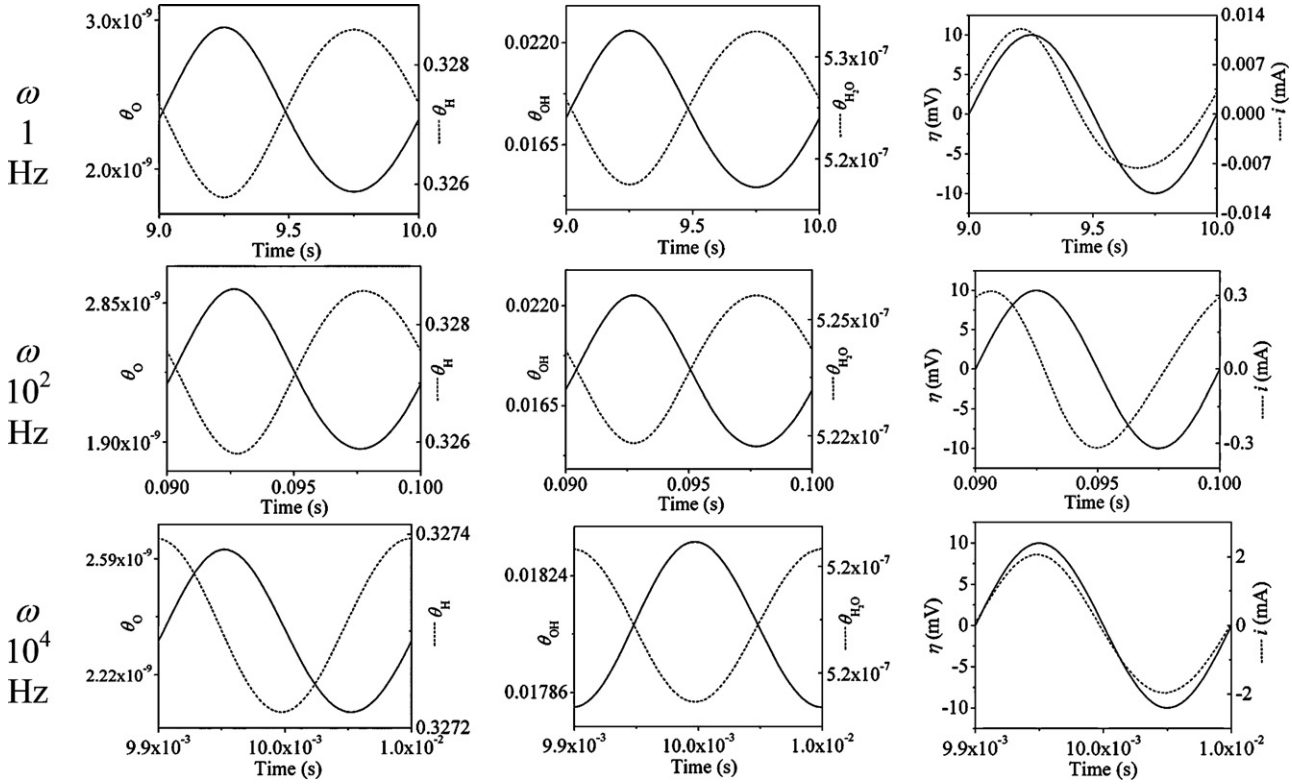

Fig. 4. Steady state dynamic response of the system to sinusoidal varying input over-voltage at three different frequencies.

about their steady state values for 1 Hz and 100 Hz input frequencies. At higher frequency (10,000 Hz) this trend is maintained but the magnitude of the variation is smaller. The very little variation of H and H_2O about their steady states compared to the larger variation of O and H, observed in this work, was also reported in Bessler (2005).

The concept of the degree of rate control as defined in Eq. (36) is used to identify the RDS. This analysis was done by omitting the time varying part of the input over-voltage and retaining only the constant part (refer to Eq. (24)). The values of the system output (*i.e.*, current) were used in the calculations after it was allowed to settle down to a steady state. The degree of rate control (X_i) for all the six reactions comprising the SOFC anodic reaction mechanism are shown in Fig. 5 as functions of the over-voltage. It can be seen from Fig. 5 that the degree of rate control for the reaction given in Eq. (4) (which is a surface reaction) is the highest across the entire range of over-voltages. Therefore, this reaction seems to control the overall rate of the SOFC anodic reaction mechanism. This is followed by the surface reaction given in Eq. (5), for which the degree of rate control is high at lower over-voltages. The degree of rate control of the charge transfer reaction (Eq. (2)) increases at higher over-voltages (*i.e.*, at higher current). The degree of rate control for the adsorption/desorption reactions (Eqs. (6) and (7)) remain close to zero over the entire range of the over-voltages. The above analysis suggests that the surface reactions may have a greater role in deciding the overall rate of the SOFC anodic Ni, H_2–H_2O|YSZ reaction mechanism. It is interesting to note that a surface reaction was predicted to be rate determining in the case of SOFC anodic reactions in Yoon, Gopalan, and Pal (2007).

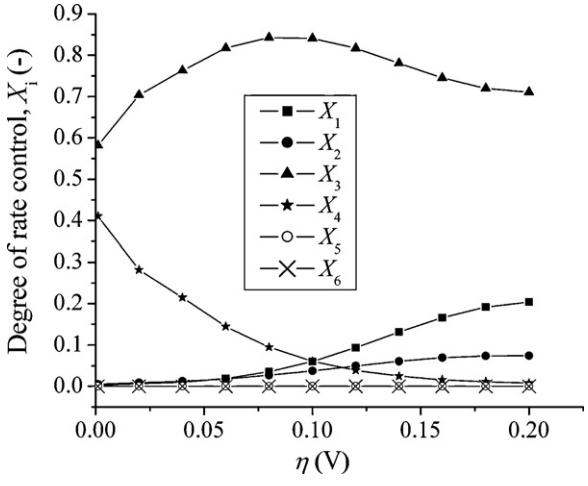

Fig. 5. The degree of rate control of the six steps in the SOFC anodic reaction mechanism as a function of the over-voltage.

8. Conclusions

The traditional kinetic modeling of chemical reaction mechanisms suffer from the drawback that the thermodynamics is not integrated into its structure. If the reaction mechanism contains a loop, the estimated reaction rate constants using such a model will violate the Wegscheider condition and hence results in the violation of microscopic reversibility.

If the driving forces and fluxes are integrated into the structure of the model, then their sign equivalence will alone ensure that thermodynamics is not violated. However, the quantities usually considered as potentials and driving forces of chemical reaction systems (chemical potentials and Gibbs free energies respectively) are quite unsuited for kinetic modeling far from equilibrium. Therefore, in this work, the concept of thermo-kinetic force proposed in Ederer and Gilles (2007a), which has the same sign dependence on the concentrations as the Gibbs free energy, is used for modeling anodic Ni, H_2–H_2O|YSZ electrochemical reaction kinetics.

It is shown that the parameter estimation using the modeling method proposed in Ederer and Gilles (2007a) can be performed iteratively by means of exploiting the relation between the reaction rate constants and the set of capacities of a reaction and also the Wegscheider condition. This procedure effectively fits not only the reaction resistances but also the capacities to the experimental data and results in parameter estimates, which do not cause the model to violate the laws of thermodynamics. Further, the identification of the RDS in the mechanism is done using the concept of the 'Degree of rate control'.

The forward and the reverse reaction rate constants for the surface reactions (Eqs. (4) and (5)) were found to be violating the condition in Eq. (54) in Appendix B. Therefore, the corresponding reaction resistances were estimated using the iterative parameter estimation procedure, of which, two iterations were performed. Using these parameters, the Bode and Nyquist plots for the impedances are obtained from the simulations. The least squares error between the simulated and experimental impedances is found to be less than that of other models in literature. The dynamic response curves for the surface coverage fractions and current also show reasonable trends. Using the concept of the 'Degree of rate control', it is found that the surface reactions (especially the reaction in Eq. (4)) may have a greater role in deciding the overall rate of the SOFC anodic Ni, H_2–H_2O|YSZ reaction mechanism.

Thus the iterative parameter estimation procedure, which utilizes the revised formulation of the physicochemical model of the SOFC anodic Ni, H_2–H_2O|YSZ reaction mechanism results in reaction rate constant estimates that do not violate the thermodynamic consistency of the system. This parameter estimation procedure using the revised model formulation may also be adapted for other complex chemical and biochemical reaction networks for which the reaction rate constants need to be estimated using the experimental data.

These authors have developed bond graph models (Dauphin-Tanguy, 2000; Mukherjee, Karmakar, & Samantaray, 2006; Thoma & Ould Bouamama, 2000) and model-based control strategies for SOFC systems (Vijay, Samantaray, & Mukherjee, 2008; Vijay, Samantaray, & Mukherjee, 2009a; Vijay, Samantaray, & Mukherjee, 2009b; Vijay, Samantaray, & Mukherjee, 2010). Those models use simplified formulations of the overall anodic reaction dynamics. There is abundant literature on bond graph modeling of chemical reactions (Couenne, Jallut, Lefèvre, Gorrec, & Maschke, 2007; Couenne, Jallut, Maschke, Tayakout, & Breedveld, 2008; Lamamra, Khemliche, & Khellaf, 2006; Thoma & Ould Bouamama, 2000) and fuel cell systems (Saisset, Fontes, Turpin, & Astier, 2006) where both pseudo and true bond graph formulations have been used. However, those models are easily computable because the micro-kinetics of the reaction is not considered. An integrated and accurate model of the total SOFC system would be extremely stiff due to the large differences between the time scales of different separate dynamically interacting parts. That is why a multi-scale modeling approach is required (Franco, Jallut, & Maschke, 2006; Franco, Schott, Jallut, & Maschke, 2007). We will develop such a multi-scale bond graph model in our future work.

Moreover, bond graph models give an energetically consistent platform for parameter identification (Delgado & Garcia, 1993). One can perform partial system identification very easily from available time domain experimental data by using the concept of sensitivity bond graphs (Gawthrop, 2000; Gawthrop & Ronco, 2000). Our future work will also address these issues.

Appendix A.

In this appendix, it is shown that adopting the quantities usually considered as potentials and driving forces of a chemical reaction system (μ and ΔG) for modeling reaction systems far from equilibrium will result in computational difficulties. For the sake of the discussion, let us consider the reaction, $A \underset{k_-}{\overset{k_+}{\rightleftharpoons}} B$. Assuming ideal mixtures, the chemical potentials of the reactant and product species are given as

$$\mu_A = \mu_{A,0} + RT\ \ln(c_A) \tag{37}$$

and

$$\mu_B = \mu_{B,0} + RT \ln(c_B), \tag{38}$$

where the reference concentrations are assumed to be unity. The concentrations of 'A' and 'B' are obtained from Eqs. (37) and (38) respectively as

$$c_A = \exp\left(\frac{\mu_A - \mu_{A,0}}{RT}\right) \tag{39}$$

and

$$c_B = \exp\left(\frac{\mu_B - \mu_{B,0}}{RT}\right). \tag{40}$$

The reaction flux for the reaction considered is given by

$$J = k_+ c_A - k_- c_B. \tag{41}$$

Substituting Eqs. (39) and (40) into Eq. (41), we get

$$J = k_+ \exp\left(\frac{\mu_A - \mu_{A,0}}{RT}\right) - k_- \exp\left(\frac{\mu_B - \mu_{B,0}}{RT}\right). \tag{42}$$

The reaction resistance is given by

$$R = \frac{\Delta G}{J} = \frac{|\nu_A|\mu_A - |\nu_B|\mu_B}{k_+ \exp((\mu_A - \mu_{A,0})/RT) - k_- \exp((\mu_B - \mu_{B,0})/RT)}, \tag{43}$$

which is highly non-linear and cannot be approximated by a constant value if the simulations of the system far from equilibrium are required. In contrast, the new formulation reaction resistance is constant and simulations of the system far from equilibrium conditions are not computationally taxing.

Appendix B.

The thermodynamic kinetic modeling (Ederer & Gilles, 2007a) of a general surface reaction in terms of surface coverage fractions is given in this appendix. It is also shown that this formulation satisfies the De Donder relations.

The chemical potential of a component 'j' in an ideal mixture is given as

$$\mu_j = \mu_{j,0}(T, p) + RT \ln\left(\frac{c_j}{c_\Sigma}\right), \tag{44}$$

where c_j is the concentration of the component 'j' and c_Σ is the reference concentration, which is usually taken as unity and $\mu_{j,0}$ is the standard chemical potential. The expression for the chemical potential can be written in terms of the dimensionless surface coverage fractions by multiplying and dividing the total number of surface sites (N_0) (refer to Eq. (15)) into the logarithmic term in Eq. (44) as

$$\mu_j = \mu_{j,0}(T, p) + RT \ln\left(\frac{\theta_j}{\theta_\Sigma}\right). \tag{45}$$

Eq. (45) can be rewritten as

$$\mu_j = RT\ \ln\left(\exp\left(\frac{\mu_{j,0}(T, p)}{RT}\right)\right) + RT\ \ln\left(\frac{\theta_j}{\theta_\Sigma}\right), \tag{46}$$

which after rearrangement gives

$$\mu_j = RT \ln\left(\frac{\theta_j}{\theta_\Sigma \exp(-\mu_{j,0}(T, p)/(RT))}\right). \tag{47}$$

Denoting $\theta_\Sigma \exp(-\mu_{j,0}(T,p)/RT) = \Theta_j$ gives

$$\mu_j = RT \ln\left(\frac{\theta_j}{\Theta_j}\right). \tag{48}$$

The ratio θ_j/Θ_j is designated as ξ_j, which may be considered to be analogous to the potential in electrical systems. Therefore, the Θ_j's which relate the potential and the generalized charges (θ_j's) (see Ederer & Gilles, 2007b for analogy with electrical circuits) are called capacities.

It is desired to derive a new driving force for the chemical reaction from $(\Delta G)_i$, which retains its sign dependence on the surface coverage fractions. The driving force for the reaction is given as

$$(\Delta G)_i = \sum_{j\in P}|\nu_j|\mu_j - \sum_{j\in R}|\nu_j|\mu_j. \tag{49}$$

Substituting the expression for the chemical potential as given in Eq. (48) into Eq. (49) gives

$$-(\Delta G)_i = RT\sum_{j\in R}|\nu_j|\ln\left(\frac{\theta_j}{\Theta_j}\right) - RT\sum_{j\in P}|\nu_j|\ln\left(\frac{\theta_j}{\Theta_j}\right). \tag{50}$$

Dividing both the sides of Eq. (50) by 'RT' and taking exponential on both sides gives the driving force $(F_d)_i$ for the reaction as

$$(F_d)_i = \exp\left(-\frac{(\Delta G)_i}{RT}\right) = \prod_{j\in R}\left(\frac{\theta_j}{\Theta_j}\right)^{|\nu_j|} - \prod_{j\in P}\left(\frac{\theta_j}{\Theta_j}\right)^{|\nu_j|}. \tag{51}$$

As the performed operations do not alter the sign of the force, the sign dependence of the new driving force $(F_d)_i$ (refer to Eq. (51)) on the surface coverage fractions is the same as the sign dependence of $(\Delta G)_i$ (refer to Eq. (49), where μ_j is given by Eq. (45)) on the surface coverage fractions. Now, a reaction resistance is defined such that the reaction flux is given by, $J_i = R_i^{-1}(F_d)_i$.

$$J_i = R_i^{-1}(F_d)_i = R_i^{-1}\prod_{j\in R}\theta_j^{|\nu_j|}\Theta_j^{-|\nu_j|} - R_i^{-1}\prod_{j\in P}\theta_j^{|\nu_j|}\Theta_j^{-|\nu_j|}. \tag{52}$$

The reaction flux defined by the traditional modeling formalism, is given as

$$J_i = k_{+i}\prod_{j\in R}\theta_j^{|\nu_j|} - k_{-i}\prod_{j\in P}\theta_j^{|\nu_j|}. \tag{53}$$

The reaction flux in Eq. (52) will be equal to the reaction flux given by the mass action law in Eq. (53) only if the reaction resistance R_i is defined as

$$R_i = k_{+i}^{-1}\prod_{j\in R}\Theta_j^{-|\nu_j|} = k_{-i}^{-1}\prod_{j\in P}\Theta_j^{-|\nu_j|}. \tag{54}$$

Thus, the driving force for the reaction is redefined such that it retains the sign dependence on the surface coverage fractions. As a result, a constant reaction resistance (R_i) is also obtained.

Any set of equilibrium surface coverage fractions (θ_j's) can be used as the capacities (Θ_j's) as shown in the following. At thermodynamic equilibrium, the Gibbs free energy for any reaction must be zero. Therefore:

$$(\Delta G)_i = \sum_{j\in P}|\nu_j|\mu_j - \sum_{j\in R}|\nu_j|\mu_j = 0. \tag{55}$$

Substituting Eq. (48) into Eq. (55) and with some algebraic manipulations we get

$$\ln\left(\frac{\prod_{j\in P}\theta_{j,\text{eq}}^{|\nu_j|}}{\prod_{j\in R}\theta_{j,\text{eq}}^{|\nu_j|}}\right) = \ln\left(\frac{\prod_{j\in P}\Theta_j^{|\nu_j|}}{\prod_{j\in R}\Theta_j^{|\nu_j|}}\right) = \ln(K_{\text{eq}}), \tag{56}$$

where K_{eq} is the equilibrium constant of the reaction. The condition expressed by Eq. (56) is applicable to all the reactions in the SOFC anodic reaction mechanism. From Eq. (56), it is evident that any set of equilibrium surface coverage fractions (θ_j's) of the system can be used as capacities.

The thermodynamic consistency of this formulation is maintained even for simulations far from equilibrium. This is because; it satisfies the De Donder equation as shown in the following. The ratio of the forward and reverse reaction fluxes is given as

$$\frac{J_{+i}}{J_{-i}} = \frac{k_{+i}\prod_{j\in R}\theta_j^{|\nu_j|}}{k_{-i}\prod_{j\in P}\theta_j^{|\nu_j|}}. \tag{57}$$

If c_Σ is unity in Eq. (44), then Eq. (45) becomes

$$\mu_j = \mu_{j,0} + RT\ln\theta_j, \tag{58}$$

which on rearrangement gives

$$\theta_j = \exp\left(\frac{\mu_j - \mu_{j,0}}{RT}\right). \tag{59}$$

Substitution of Eq. (59) into Eq. (57) gives

$$\frac{J_{+i}}{J_{-i}} = \frac{k_{+i}\prod_{j\in R}\exp(((\mu_j-\mu_{j,0})\nu_j)/RT)}{k_{-i}\prod_{j\in P}\exp(((\mu_j-\mu_{j,0})\nu_j)/RT)} = \frac{k_{+i}\exp\left(\sum_{j\in R}\mu_j\nu_j/RT\right)\exp\left(-\sum_{j\in R}\mu_{j,0}\nu_j/RT\right)}{k_{-i}\exp\left(\sum_{j\in P}\mu_j\nu_j/RT\right)\exp\left(-\sum_{j\in P}\mu_{j,0}\nu_j/RT\right)}, \tag{60}$$

which can be rearranged to get

$$\frac{J_{+i}}{J_{-i}} = \frac{k_{+i}}{k_{-i}}\exp\left(\frac{\sum_{j\in R}\mu_j\nu_j - \sum_{j\in P}\mu_j\nu_j}{RT}\right)\exp\left(\frac{\sum_{j\in P}\mu_{j,0}\nu_j - \sum_{j\in R}\mu_{j,0}\nu_j}{RT}\right), \tag{61}$$

which further gives

$$\frac{J_{+i}}{J_{-i}} = \frac{k_{+i}}{k_{-i}}\exp\left(-\frac{(\Delta G)_i}{RT}\right)\exp\left(\frac{(\Delta G^0)_i}{RT}\right), \tag{62}$$

where $(\Delta G^0)_i$ is the Gibbs free energy of the reaction at standard state.

From Eq. (56), the equilibrium ratio of the reaction rate constants is given by

$$\frac{k_{+i}}{k_{-i}} = \frac{\prod_{j\in P}\theta_{j,\text{eq}}^{|\nu_j|}}{\prod_{j\in R}\theta_{j,\text{eq}}^{|\nu_j|}}. \tag{63}$$

By substituting Eq. (45) into Eq. (55), it can be deduced that

$$\exp\left(-\frac{(\Delta G^0)_i}{RT}\right) = \frac{\prod_{j\in P}\theta_{j,\text{eq}}^{|\nu_j|}}{\prod_{j\in R}\theta_{j,\text{eq}}^{|\nu_j|}} = \frac{k_{+i}}{k_{-i}}. \tag{64}$$

Substitution of Eq. (64) into Eq. (62) gives

$$\frac{J_{+i}}{J_{-i}} = \exp\left(-\frac{(\Delta G)_i}{RT}\right) = \exp\left(-\frac{(\mathrm{d}G/\mathrm{d}\xi)_i}{RT}\right), \tag{65}$$

which is the De Donder equation, where ξ is the reaction advancement coordinate. Therefore, the satisfaction of the condition in Eq. (54), which is ensured through the introduction of the reaction resistance in the new formulation (refer to Eqs. (54) and (56)), also results in the satisfaction of the De Donder equation and hence ensures thermodynamic consistency of the reaction system for simulations far from equilibrium.

References

Avetisov, A. K., Kuchaev, V. L., & Murzin, D. Y. (2006). Thermodynamic analysis of reaction schemes with empty routes. *AIChE Journal*, *52*(12), 4273–4275.

Baranski, A. (1999). On the usefulness of Campbell's concept of the rate-determining step. *Solid State Ionics*, *117*, 123–128.
Bessler, W. G. (2005). A new computational approach for SOFC impedance from detailed electrochemical reaction–diffusion models. *Solid State Ionics*, *176*, 997–1011.
Bessler, W. G., Gewies, S., & Vogler, M. (2007). A new framework for physically based modeling of solid oxide fuel cells. *Electrochimica Acta*, *53*, 1782–1800.
Bessler, W. G., Warnatz, J., & Goodwin, D. G. (2007). The influence of equilibrium potential on the hydrogen oxidation kinetics of SOFC anodes. *Solid State Ionics*, *177*, 3371–3383.
Bieberle, A. (2000). *The electrochemistry of solid oxide fuel cell anodes: Experiments, modeling, and simulations*. Ph.D. Thesis. Zürich, Switzerland: Swiss Federal Institute of Technology.
Bieberle, A., & Gauckler, L. J. (2002). State-space modeling of the anodic SOFC system Ni, H_2–H_2O|YSZ. *Solid State Ionics*, *146*, 23–41.
Bijlsma, S., Boelens, H. F. M., Hoefsloot, H. C. J., & Smilde, A. K. (2000). Estimating reaction rate constants: Comparison between traditional curve fitting and curve resolution. *Analytica Chimica Acta*, *419*, 197–207.
Bockris, J. O'M., & Reddy, A. K. N. (1973). *Modern electrochemistry: An introduction to an interdisciplinary area*. Springer.
Boudart, M. (2001). Kinetic generalities in catalysis. *Topics in Catalysis*, *14*(1–4), 181–185.
Boudart, M., & Tamaru, K. (1991). The step that determines the rate of a single catalytic cycle. *Catalysis Letters*, *9*, 15–22.
Campbell, C. T. (1994). Micro- and macro-kinetics: Their relationship in heterogeneous catalysis. *Topics in Catalysis*, *1*, 353–366.
Campbell, C. T. (2001). Finding the rate-determining step in a mechanism. *Journal of Catalysis*, *204*, 520–524.
Colquhoun, D., Dowsland, K. A., Beato, M., & Plested, A. J. R. (2004). How to impose microscopic reversibility in complex reaction mechanisms. *Biophysical Journal*, *86*, 3510–3518.
Couenne, F., Jallut, C., Lefèvre, L., Gorrec, Y. L., & Maschke, B. (2007). Basis for bond-graph modeling in chemical engineering. *Computer Aided Chemical Engineering*, *24*, 69–74.
Couenne, F., Jallut, C., Maschke, B., Tayakout, M., & Breedveld, P. (2008). Structured modeling for processes: A thermodynamical network theory. *Computers and Chemical Engineering*, *32*(6), 1128–1142.
Dauphin-Tanguy, G. (2000). *Les Bond graphs*. Paris: Hermes Science Europe Ltd.
Delgado, M., & Garcia, J. (1993). Parametric identification on bond graph models. In *Proceedings of the IEEE international conference on systems, man and cybernetics, vol. 1* Le Touquet, France, (pp. 583–587).
Dumesic, J. A. (1999). Analyses of reaction schemes using De Donder relations. *Journal of Catalysis*, *185*, 496–505.
Ederer, M., & Gilles, E. D. (2007a). Thermodynamically feasible kinetic models of reaction networks. *Biophysical Journal*, *92*, 1846–1857.
Ederer, M., & Gilles, E. D. (2007b). Thermodynamic-kinetic modeling and electrical engineering. In *Proceedings of the FOSBE* Stuttgart, Germany, (pp. 135–140).
Fishtik, I., Callaghan, C. A., Fehribach, J. D., & Datta, R. (2005). A reaction route graph analysis of the electrochemical hydrogen oxidation and evolution reactions. *Journal of Electroanalytical Chemistry*, *576*, 57–63.
Fishtik, I., & Datta, R. (2001). De Donder relations in mechanistic and kinetic analysis of heterogeneous catalytic reactions. *Industrial & Engineering Chemistry Research*, *40*, 2416–2427.
Franco, A. A., Jallut, C., & Maschke, B. (2006). A multi-scale dynamic mechanistic model for transient analysis of PEFCs. In *Proceedings of the 16th world hydrogen energy conference* Lyon, France.
Franco, A. A., Schott, P., Jallut, C., & Maschke, B. (2007). A multi-scale dynamic mechanistic model for the transient analysis of PEFCs. *Fuel Cells*, *7*(2), 99–117.
Gawthrop, P. J. (2000). Sensitivity bond graphs. *Journal of the Franklin Institute*, *337*(7), 907–922.
Gawthrop, P. J., & Ronco, E. (2000). Estimation and control of mechatronic systems using sensitivity bond graphs. *Control Engineering Practice*, *8*(11), 1237–1248.
Holstein, W. L., & Boudart, M. (1997). Application of the De Donder relation to the mechanism of catalytic reactions. *Journal of Physical Chemistry B*, *101*, 9991–9994.
Lamamra, A., Khemliche, M., & Khellaf, A. (2006). Bond graph modeling of a chemical reactor. *WSEAS Transactions on Computers*, *5*(1), 223–228.
Macdonald, J. R. (1987). *Impedance spectroscopy*. New York: John Wiley & Sons, Inc.
Mhadeshwar, A. B., Wang, H., & Vlachos, D. G. (2003). Thermodynamic consistency in microkinetic development of surface reaction mechanisms. *Journal of Physical Chemistry B*, *107*, 12721–12733.
Mitterdorfer, A., & Gauckler, L. J. (1998). $La_2Zr_2O_7$ formation and oxygen reduction kinetics of the $La_{0.85}Sr_{0.15}Mn_yO_3$, O_2(g)|YSZ system. *Solid State Ionics*, *111*, 185–218.
Mitterdorfer, A., & Gauckler, L. J. (1999a). Identification of the reaction mechanism of the Pt, O_2(g)|yttria-stabilized zirconia system. Part I. General framework, modelling, and structural investigation. *Solid State Ionics*, *117*, 187–202.
Mitterdorfer, A., & Gauckler, L. J. (1999b). Identification of the reaction mechanism of the Pt, O_2(g)|yttria-stabilized zirconia system. Part II. Model implementation, parameter estimation, and validation. *Solid State Ionics*, *117*, 203–217.
Mukherjee, A., Karmakar, R., & Samantaray, A. K. (2006). *Bond graph in modeling, simulation and fault identification* (2nd ed.). FL: CRC Press.
Onsager, L. (1931a). Reciprocal relations in irreversible processes I. *Physical Review*, *37*, 405–426.
Onsager, L. (1931b). Reciprocal relations in irreversible processes II. *Physical Review*, *38*, 2265–2279.
Qian, H., & Beard, D. A. (2005). Thermodynamics of stoichiometric biochemical networks in living systems far from equilibrium. *Biophysical Chemistry*, *114*, 213–220.
Saisset, R., Fontes, G., Turpin, C., & Astier, S. (2006). Bond graph model of a PEM fuel cell. *Journal of Power Sources*, *156*(1), 100–107 (special issue).
Thoma, J., & Ould Bouamama. (2000). *Modelling and simulation in thermal and chemical engineering: A bond graph approach*. Berlin: Springer-Verlag.
Vijay, P., Samantaray, A. K., & Mukherjee, A. (2008). Bond graph model of a solid oxide fuel cell with a C-field for mixture of two gas species. *Proceedings of IMechE Part I: Journal of Systems and Control Engineering*, *222*(4), 247–259.
Vijay, P., Samantaray, A. K., & Mukherjee, A. (2009a). On the rationale behind constant fuel utilization control of solid oxide fuel cells. *Proceedings of IMechE Part I: Journal of Systems and Control Engineering*, *223*(2), 229–252.
Vijay, P., Samantaray, A. K., & Mukherjee, A. (2009b). A bond graph model-based evaluation of a control scheme to improve the dynamic performance of a solid oxide fuel cell. *Mechatronics*, *19*(4), 489–502.
Vijay, P., Samantaray, A. K., & Mukherjee, A., (2010). Constant fuel utilization operation of a SOFC system: An efficiency viewpoint. *ASME Journal of Fuel Cell Science and Technology*, 7(2), doi:10.1115/1.4000631.
Yang, J., Bruno, W. J., Hlavacek, W. S., & Pearson, J. E. (2006). On imposing detailed balance in complex reaction mechanisms. *Biophysical Journal*, *91*(3), 1136–1141.
Yoon, K. J., Gopalan, S., & Pal, U. B. (2007). Effect of fuel composition on performance of single-step cofired SOFCs. *Journal of the Electrochemical Society*, *154*(10), B1080–B1087.